full papers

Length Distribution of Single-Walled Carbon Nanotubes in Aqueous Suspension Measured by Electrospray Differential Mobility Analysis

Leonard F. Pease III, De-Hao Tsai, Jeffery A. Fagan, Barry J. Bauer, Rebecca A. Zangmeister, Michael J. Tarlov, and Michael R. Zachariah*

The first characterization of the length distribution of single-walled carbon nanotubes (SWCNT) dispersed in a liquid by electrospray differential mobility analysis (ES-DMA) is presented. Although an understanding of geometric properties of SWCNTs, including length, diameter, aspect ratio, and chirality, is essential for commercial applications, rapid characterization of nanotube length distributions remains challenging. Here the use of ES-DMA to obtain length distributions of DNA-wrapped SWCNTs dispersed in aqueous solutions is demonstrated. Lengths measured by ES-DMA compare favorably with those obtained from multiangle light scattering, dynamic light scattering, field flow fractionation with UV/vis detection, and atomic force microscopy, validating ES-DMA as a technique to measure SWCNTs of <250 nm in length. The nanotubes are previously purified and dispersed by wrapping with oligomeric DNA in aqueous solution and centrifuging to remove bundles and amorphous carbon. These dispersions are particularly attractive due to their amenability to bulk processing, ease of storage, high concentration, compatibility with biological and high-throughput manufacturing environments, and for their potential applications ranging from electronics and hydrogen-storage vessels to anticancer agents.

Keywords:
- aqueous suspensions
- carbon nanotubes
- electrospray differential mobility analysis
- length distribution
- scanning mobility

1. Introduction

Single-walled carbon nanotubes (SWCNTs) hold great potential as components in a variety of applications including electronics, nanolasers, hydrogen-storage vessels, sensors, and anticancer therapeutics due to their outstanding mechanical, electrical, and optical properties.[1–8] Characterization of the SWCNT length distribution is important for several of these applications. For example, Kam et al. demonstrated SWCNTs modified with proteins to be potential anticancer treatments, and Becker et al. showed the uptake of SWCNTs into cells to depend on length with nanotubes of <200 nm in length incorporated more readily.[4,9] Similarly, Barone et al. used fluorescence from SWNCTs and glucose oxidase as a blood-sugar sensor, and Fagan et al. recently demonstrated that the optical intensity (e.g., UV/vis and fluorescence) of SWCNTs increases with nanotube length.[2,10] Likewise, CNT-based transparent

[*] Dr. D.-H. Tsai, Prof. M. R. Zachariah
The University of Maryland
College Park, MD 20742 (USA)
E-mail: mrz@umd.edu
Prof. L. F. Pease III,+ Dr. D.-H. Tsai, Dr. J. A. Fagan, Dr. B. J. Bauer, Dr. R. A. Zangmeister, Dr. M. J. Tarlov, Prof. M. R. Zachariah
National Institute of Standards and Technology
Gaithersburg, MD 20899 (USA)

[+] Current address:
University of Utah
50 South Central Campus Drive
Rm. 3290 MEB
Salt Lake City, UT 84112 (USA)

Supporting Information is available on the WWW under http://www.small-journal.com.

electrodes may replace indium tin oxide due to their improved flexibility, and the mechanical properties of nanotube-reinforced composites will likely depend on the SWCNT length distribution.[11,12]

The average length of nanotubes in a bulk sample has been measured in several ways. For instance, multiangle light scattering (MALS) measures the intensity and angular dependence of scattered light to produce an average rod length and molar mass.[2,13,14] Dynamic light scattering (DLS) measures the diffusion of rods and rheological models are then used to produce average lengths. Both of these methods produce ensemble-average lengths of broad distributions and often estimate the nanotubes to be rigid rods having a monodisperse, monomodal length distribution.[13,14] However, nanotube populations encountered in practice are often best described by polydisperse distributions that can be harder to quantify. To estimate the polydispersity, Bauer et al. calculated the polydispersity index (PDI) from MALS data for SWCNTs, supposing a bimodal distribution of nanotube lengths.[2,9,13,14] Even so, the accuracy of optical scattering techniques decreases as the SWCNT length shrinks (i.e., <200 nm).

The polydispersity can be narrowed, at least partially, by first separating the SWCNTs with field flow fractionation (FFF) or by fractionating the sample with size-exclusion chromatography (SEC).[2,13,15] Calibration with known standards allows conversion of the elution times to length distributions. For instance, Chun et al. found FFF with UV/vis detection to be useful for extracting average SWCNT lengths when suitably calibrated using latex spheres.[13]

Alternatively, the distribution of lengths can be measured by microscopy techniques such as atomic force microscopy (AFM), scanning electron microscopy (SEM), or transmission electron microscopy (TEM). Image analysis can then be used to assemble histograms of the nanotube length distribution. Microscopy methods, however, typically only analyze a relatively small fraction of the total sample of SWCNTs, are time consuming, often taking days instead of minutes, and may be prone to bias due to heterogeneity in the spatial distribution or visibility of the SWCNTs on the substrate.

Here we use differential mobility analysis (DMA) to rapidly obtain length distributions of SWCNTs shorter than 250 nm. DMA possesses several advantages relative to other methods (e.g., AFM, MALS, etc.) including 1) speed ($\approx$10–50 minutes per analysis), 2) resolution as low as $\approx$0.2 nm,[16,17] 3) direct reporting of statistically precise multimodal distributions of SWCNTs, 4) calibration standards are unnecessary to determine the size, and 5) negligible thermal heating. In this method SWCNTs are first aerosolized, charged, and then classified in the DMA (see Figure 1) according to their ion mobility, which is determined by electrical and aerodynamic drag forces acting on the SWCNTs. Essentially, the DMA acts as a band-pass filter selecting SWCNTs with a narrow band of charge-to-size ratios for counting with a condensation particle counter (CPC). Within the CPC, size-selected SWCNTs transit a saturated butanol vapor, heterogeneously nucleating micrometer-sized droplets, which are counted electronically as they individually block a laser beam. An entire distribution is obtained by sweeping the voltage applied to the DMA and counting the number of nanotubes with the corresponding charge-to-size ratio. The voltage at which
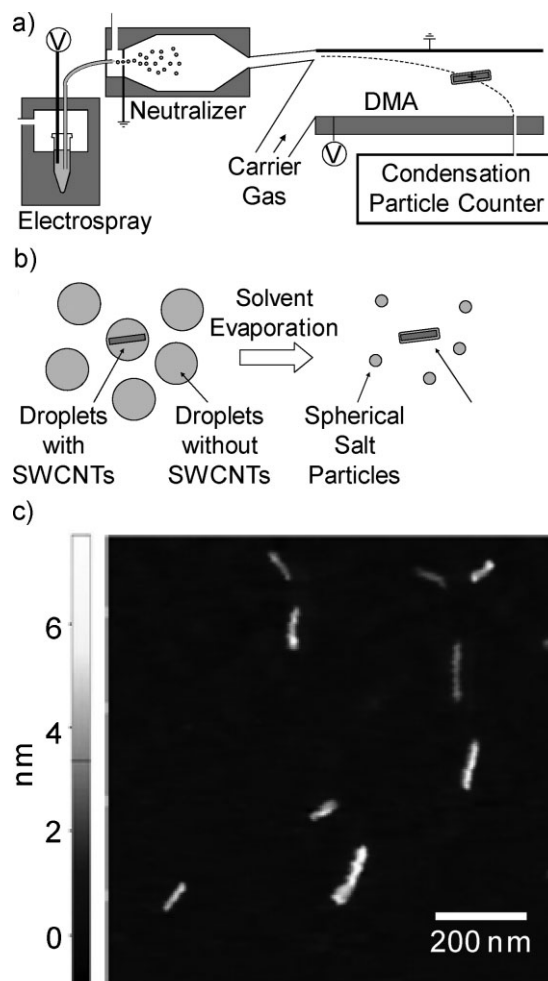
Figure 1. a) Diagram of experimental system including an electrospray system to sample from liquid suspension, a DMA that acts as a narrow band-pass filter separating particles based on their charge-to-size ratio, and a CPC that counts selected particles. b) Schematic image depicting electrospray droplets containing dilute non-volatile salts, some of which contain SWCNTs. The droplets dry leaving spherical salt particles and individual SWCNTs coated with non-volatile residue. c) Topographical AFM image (non-contact mode) of SWCNTs electrosprayed onto a freshly cleaved mica surface using an electrostatic deposition chamber. This image shows that salt-encrusted SWCNTs retain a linear shape; mean heights of the individual nanotube features calculated using grain analysis software ranged from 1.9 nm to 3.8 nm.

particles are detected can be related to a spherically equivalent diameter, termed the mobility diameter.

To obtain lengths for axially symmetric tubes and rods, models for the aerodynamic drag acting on the SWCNTs are necessary, such as those for right circular cylinders and prolate spheres derived by Song et al. and Dahneke et al.[18,19] The DMA provides only one length scale so a diameter must be selected to determine a length. Recently, Kim et al., using Dahneke's model for a cylinder, accounted for the rotation and alignment of nanowires due to electrical forces during their flight within a DMA.[20] By accounting for the competition between electrically induced alignment and Brownian-induced randomization, which depends on nanotube length, they were able to develop an analysis of nanowire transport through a

DMA, which enables a direct determination of length. This approach was used to probe nanotube growth kinetics.[21] We adapt this model to determine the length distribution of SWCNTs dispersed in aqueous solution.

Although the Zachariah and Kauppinen groups have previously demonstrated the use of DMA to characterize SWCNTs or multi-walled (MW) CNTs produced in the gas phase, to our knowledge the work presented here is the first use of DMA to characterize nanotubes processed in liquid suspensions.[20,22–24] Aqueous dispersions of SWCNTs are of considerable technological interest because of the relatively high concentration and dispersion that can be achieved in these systems, their environmental friendliness, their stability in storage, and their compatibility with biological and high-throughput manufacturing environments.[25]

In order to measure the size of aqueously dispersed SWCNTs with DMA, the nanotubes must first be transferred from the solution to the gas phase. This process is accomplished using electrospray. The electrospray uses only 10 µL of solution per analysis to produce a steady stream of highly charged, monodisperse droplets, some of which contain an individual nanotube. These droplets then pass into a bipolar charge neutralizer where the droplet dries, leaving an aerosolized nanotube (see Figure 1). The neutralizer is also a bipolar charger that affixes a charge state of $+1, 0$, or -1 to the SWCNTs according to a modified Boltzmann distribution.[26,27] By fixing the charge of the SWCNTs with the neutralizer and separating the nanotubes in the DMA based on their charge-to-size ratio, the size distribution of SWCNTs is obtained.

We now describe the measurement of size distributions with electrospray (ES)-DMA, detail the conversion of the raw DMA data into length distributions accounting for non-volatile residue that encrust the nanotubes, and compare lengths measured by ES-DMA with those obtained by other techniques.

2. Results and Discussion

The nanotubes analyzed in this study are commercially available SWCNTs grown through a cobalt molybdenum catalyst (CoMoCat) process. The SWCNTs were processed using the following steps. To provide optimal dispersion of individual nanotubes, the SWCNTs were wrapped in DNA as per the method of Zheng et al.[25,28,29] Individual SWCNTs were then separated through centrifugation from non-SWCNT carbon, metallic catalyst particles, and bundled SWCNTs. Finally, individual SWCNTs were fractioned using SEC into aliquots based on nanotube size.[2,9]

A key feature of our analysis is the use of electrospray. Previous efforts to analyze nanotubes with DMA have studied single- and multi-walled CNTs that were produced in the gas phase without dispersion in liquids.[19–23] Here we use electrospray sampling from liquids, which allows the DMA to size nanotubes dispersed in aqueous solution. There are two potential complications that electrospray sampling can introduce into the analysis of nanomaterials by DMA. First, if more than one nanoparticle is contained in an electrosprayed droplet then, as the droplet solvent evaporates, the nanoparticles will eventually be forced into close contact, agglomerate, and be

detected as an aggregate by the DMA. We avoid this type of spurious result by working with low solution concentrations of SWCNTs, $<100 \, \mu g \, mL^{-1}$, in conjunction with small-diameter capillaries that produce relatively small electrospray droplets ≈ 250 nm in diameter. Considering the volume of these droplets and the concentration of SWCNTs used, we estimate that statistically one or fewer SWCNTs will be in each electrosprayed droplet, indicating that the electrospray process will not produce spurious aggregates of SWCNTs.[9,30]

The second potential complication of electrospray sampling of nanomaterials is the generation of salt precipitants that can bias the DMA size measurements. The presence of salt precipitants in the electrospray process is well established[17,31–34] and was first reported by Fenn et al. in electrospray mass-spectrometry experiments.[33,34] In our experiments, this phenomenon results from the evaporation of solvent from electrosprayed droplets while they are in transit to the DMA, which causes nonvolatile species present in the electrospray buffer, primarily electrolytes, to precipitate out. Salt precipitation will occur for the two types of droplet produced by electrospraying dilute solutions of nanomaterials: those droplets without nanoparticles and those containing a nanoparticle. In the case of electrosprayed droplets containing no nanoparticles, salt particles will be produced. For droplets containing a nanoparticle, the salt will precipitate onto the surface of the nanoparticle. Recent studies of electrosprayed nanomaterials including gold nanoparticles and proteins determined that thin salt shells, a few nanometers thick, surrounded the core nanomaterial.[16,17,31,32] Additional evidence for the salt coating of nanoparticles is that the apparent size of nanoparticles measured with DMA decreases with decreasing concentration of non-volatile salts in solutions of the nanomaterials. These salt shells bias the size determination by increasing the apparent diameter of the nanomaterial. A similar phenomenon undoubtedly occurs in the ES of DNA-wrapped SWCNTs. The non-volatile species in this case includes buffer components (NaCl and Tris-HCl) and free DNA strands.[2,14,25] Fortunately, we can account for this bias because the droplets are highly uniform and reproducible in size when the electrospray is operated in the stable cone-jet mode. Each droplet is the same in size and concentration of salt thus the amount of salt that dries onto the surface of a SWCNT or into a salt particle is essentially equivalent. Thus, by measuring the diameter of the salt particle, we can determine the volume of salts that precipitates onto the SWCNTs and correct for its contribution to the apparent measured size.

2.1. Conversion of Raw Spectra to Length Distribution

Figure 2a displays typical ES-DMA data of a DNA-wrapped SWCNT sample. The plot shows the raw counts for positively charged particles obtained by the CPC versus the applied DMA voltage. The sign of the DMA voltage determines whether positively or negatively charged particles are enumerated, and the magnitude of the voltage controls the size of SWCNTs selected for counting. This voltage can be converted either to a *diameter* for spherical particles composed of nonvolatile salts or to a *length* for SWCNTs, which we

a)

b)

c)
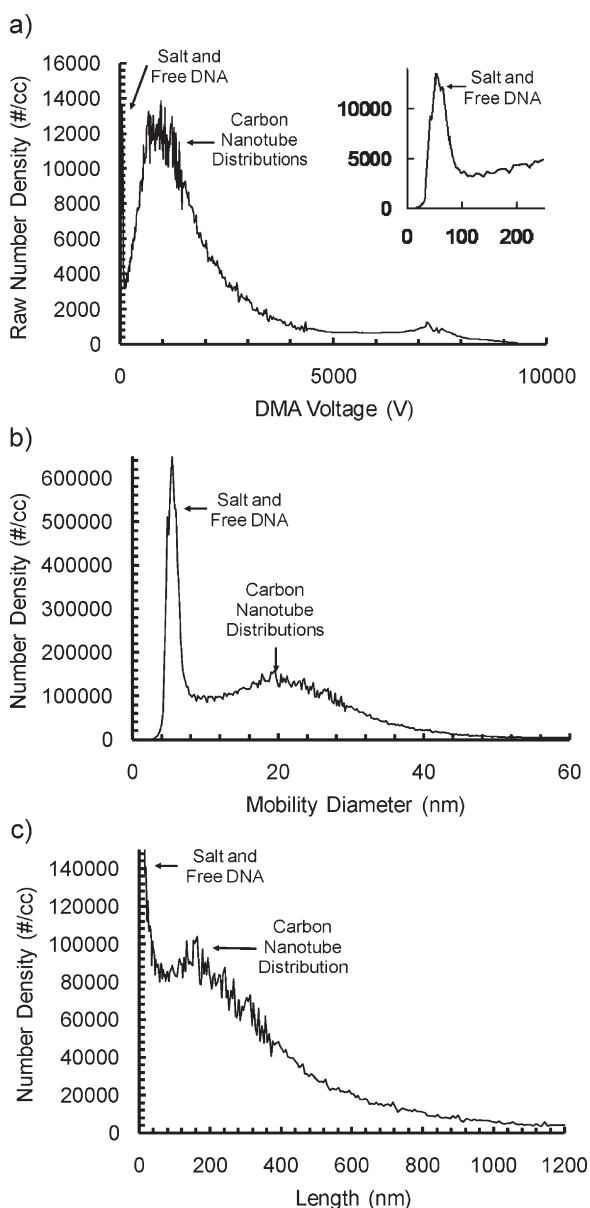
Figure 2. Distributions measured by ES-DMA of SWCNTs prior to SEC fractionation. a) Raw data displayed as the number density of positively charged particles versus the magnitude of the voltage applied to the DMA for SWCNTs. b) The data of panel (a) converted to a mobility size distribution showing the number density for all particles regardless of charge (using Equation (1)) versus the spherically equivalent mobility diameter. c) Length distribution displaying the number density of all particles regardless of charge (using Equation (2)) versus SWCNT lengths with a salt particle diameter of 5.4 nm and a diameter of DNA-wrapped SWCNTs of 2.0 nm.

demonstrate below. The ES-DMA spectrum of this sample is dominated by a broad peak between 100 V and 5000 V, a feature that corresponds to the distribution of the SWCNTs. A less prominent peak is also present between 20 V and 100 V, a feature seen more clearly in the inset of Figure 2a. As low voltages correspond to high mobility particles, this peak is assigned to particles of non-volatile salts and free DNA that form as the electrosprayed droplets evaporate. The location of this peak is related to the volume of non-volatile material per

droplet, and the sharpness of this feature suggests a narrow size distribution of electrosprayed droplets.

Our first task is to determine the amount of non-volatile salt contained in the spherical salt particles. To determine their volume, we convert the distribution of only positively charged particles versus voltage into a distribution of all particles versus diameter. This requires two corrections. First, the DMA voltage is converted into an equivalent mobility diameter, d_m, that is, the diameter of a sphere with equivalent particle mobility (see Experimental Section for further details). Second, we divide the raw counts by the fraction of positively charged particles to find the total number of particles. This fraction, f, is particle-size dependent, and Wiedersohler and Fuchs show that for spheres

$$f = 10^{\sum_{i=0}^{5} \alpha[\log(d_m/1nm)]^i} \qquad (1)$$

where a_o to a_5 are −2.3484, 0.6044, 0.4800, 0.0013, −0.1553, and 0.0320, respectively.[26] With both conversions, Figure 2b clearly shows two features. The broad feature (8 nm to 40 nm) represents the SWCNTs, while the sharp peak centered at a diameter of 5.4 nm represents the spherical salt particles, determining the volume of non-volatile components contained in an ES droplet for this distribution.[16,32] Peaks from both sources are clearly resolved, demonstrating that small spherical particles may be differentiated from SWCNTs in a manner previously seen for the measurement of larger Au nanoparticles.[16,24] This result implies that DMA may be used to distinguish catalyst particles from mature SWCNTs despite the potential for overlapping distributions.

Our second task is to determine the length of the SWCNTs. AFM imaging of electrosprayed SWCNTs on an atomically smooth mica surface reveals that the SWCNTs retain a linear shape after the non-volatile salts precipitate onto their surfaces, as depicted in Figure 1c. We therefore model the salt–SWCNT composite as an annular salt shell surrounding a cylindrical nanotube at its core. The length of the SWCNTs can significantly affect the thickness of the annular salt shell because longer SWCNTs would be expected to support thinner annuli for a constant volume of salt. Thus, we must simultaneously determine both the thickness of the annulus and the length of the nanotube. Recently Kim et al. developed a conversion from DMA voltage to length, based on Dahneke's expression for the drag on non-spherical particles in the free-molecule regime.[19,20] We build on this model, modifying it to account for the presence of a salt shell on the surface of the SWCNT.

The model for length, solved in detail in the Experimental section, relies on two parameters that vary between samples: d_{nt}, the diameter of an individual nanotube, and d_s, the diameter of a spherical salt particle. Figure 3 shows the diameter of the nanotube without a salt crust, d_{nt}, to be the more important of the two. For example, as shown in Figure 3a, an increase in d_{nt} from 1.4 to 2.0 nm for a nanotube with a mobility diameter of 20 nm results in a decrease in SWCNT length of 71 nm. The second parameter in Figure 3b is the diameter of the salt particle, d_s. The values for this parameter were determined individually for each data set, as each has a unique d_s ranging
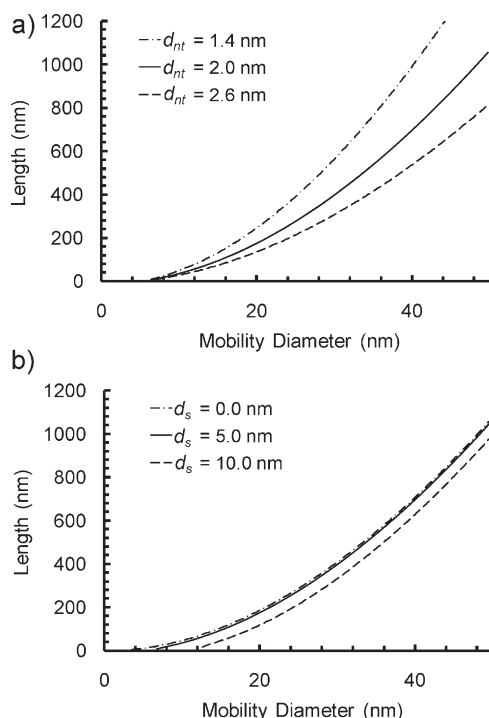
Figure 3. Length of SWCNTs versus mobility diameter as a function of the adjustable parameters d_{nt}, the diameter of an individual nanotube, and d_s, the diameter of a spherical salt particle, for a) d_{nt} values of 1.4 nm (dash dot), 2.0 nm (solid), and 2.6 nm (long dash) with $d_s = 5.0$ nm; b) for $d_s = 0.0$ nm (dash dot), 5.0 nm (solid), and 10.0 nm (long dash) with $d_{nt} = 2.0$ nm.

from 5.4 nm to 8.8 nm. Neglecting to correct for the salt crust overestimates the length of the SWCNTs by 42 nm to 56 nm.

Once we have an estimate of the length of the SWCNTs can we determine a value for the fraction of positively charged nanotubes to be used to calculate the total population of SWCNTs. The expressions for the fraction of particles with positive charges by Fuchs and Wiedersohler were developed for spheres. However, the charging probability of high aspect ratio, axisymmetric structures would be expected to differ from that of spheres due at least to an increase in field lines near sharp points. To account for this difference in charge efficiency, Wen, et al., introduced an equivalent diameter

$$D_{QE} = \frac{L_{nt}}{\ln(2L_{nt}/d_{nt})}, \tag{2}$$

for conducting, prolate spheroids.[27] They show that this equivalent diameter can be inserted into the expression of Fuchs (see Equation (1), replacing d_m with D_{QE}) to obtain the charge distribution of large-aspect-ratio particles.[35] Although developed for conducting ellipsoids, Wen et al. assert that this equivalent-diameter approach applies for dielectric ellipsoids, citing the fact that the charge distribution of Fuchs applies equally well to all spheres whether conducting or otherwise.[36] Thus, to determine the total population of SWCNTs whether positively charged or not, we determine D_{QE} using the length of the SWCNT determined above and then insert D_{QE} into the more tractable, analytical expressions of Weidersohler

(Equation (1)) to determine the fraction of positively charged SWCNTs.[26]

Figure 2c shows the length distribution, or count of all axisymmetric particles versus length, for SWCNTs prior to fractionation with SEC. The length distribution was calculated using a value of $d_{nt} = 2.0$ nm. This diameter represents the minimum measured height of the nanotube features scanned within the image shown in Figure 1c and should correspond to a nanotube with minimal salt coating. A maximum in the length distribution is observed at ≈165 nm and the full width at half maximum (FWHM) is ≈400 nm. This distribution is fairly broad, and we can observe nanotubes with lengths ranging from 30 nm to over 1000 nm. The distributions in Figure 2 were obtained in under two hours and represent the measurement of hundreds of thousands of nanotubes.

2.2. Quantification of the Average Length and Breadth of the Length Distribution

To validate the lengths found by the ES-DMA analysis, we compared ES-DMA results to those obtained by other sizing methods. For the validation studies, SWCNTs with narrower size distributions than those described above were prepared by further fractionating the SWCNTs of Figure 2 into daughter populations using SEC as described in detail elsewhere.[2] Figure 4 displays the diameter and length distributions for four of these samples. In SEC, longer tubes elute first, hence larger fraction numbers correspond to shorter tubes, a trend preserved in Figure 4b. The characteristic length of these distributions may be expressed in three ways: the mode length
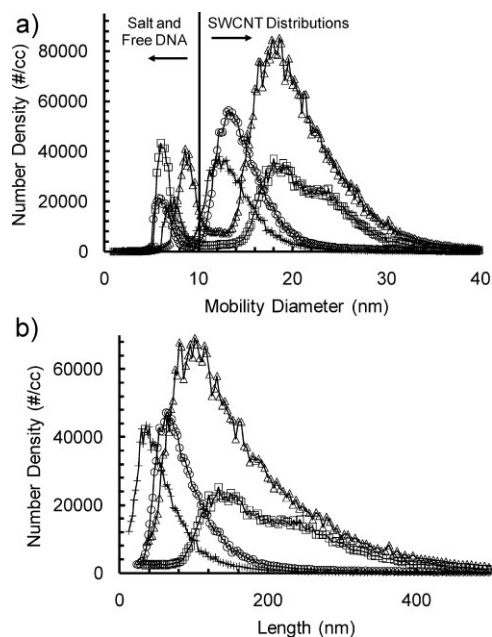
Figure 4. a) Mobility diameter and b) length distribution of SWCNTs after separation by SEC showing fractions 9 (squares), 11 (triangles), 14 (circles), and 15 (+) (see Table 1 for summary of lengths). These distributions were obtained using a 25-μm-inner-diameter electrospray capillary and a sheath flow of 30 L min⁻¹. Conversion to length takes $d_{nt} = 2.0$ nm with d_s ranging from 5.8 nm to 8.8 nm.

Table 1. Summary of the length metrics for distributions of SEC-fractionated SWCNTs.

Fraction number	L_{mode} [nm]	L_{ave} [nm]	L_{mm} [nm]	FWHM [nm]
9	133	208	254	123
10	86	150	201	106
11	81	156	213	102
12	98	136	178	74
13	88	105	124	56
14	63	94	135	56
15	36	60	97	46

(L_{mode}), the number-average length (L_{ave}), and the mass mean length (L_{mm}). The mode length corresponds to the largest number density. Table 1 summarizes the mode, L_{mode}, for each of the 7 SEC-fractionated daughter populations that we analyzed. L_{mode} is exceedingly easy to determine; however, it appears to be biased towards the shorter SWCNTs because the distributions tend to peak at shorter lengths. Perhaps a better representation of the characteristic length is the number-average length, L_{ave}, which essentially sums the lengths of all the rods and then divides by the number of rods. L_{ave} is defined as

$$L_{ave} = \frac{\sum N_i L_i}{\sum N_i} \tag{3}$$

where N_i is the number of nanotubes with a specific length, L_i. Because the conversion from DMA voltage to length does not naturally result in equally spaced length intervals, the distribution was re-sampled and binned at 5-nm increments. To eliminate any bias to L_{ave} from the salt peaks, bins smaller that the minimum between the salt and SWCNT peaks were removed before implementing Equation (3). Table 1 reports that L_{ave} ranges from 60 nm for fraction 15 up to 208 nm for fraction 9. The third metric of length is the mass mean length, L_{mm}, defined as the length for which half of the SWCNTs have a larger mass. L_{mm} is defined as

$$L_{mm} \equiv \frac{\sum m_i L_i}{\sum m_i} = \frac{\sum N_i L_i^2}{\sum N_i L_i} \tag{4}$$

where m_i is the mass of nanotubes in bin i. This may be a more appropriate length scale for comparison with mass-dependent measurement techniques. As seen in Table 1, L_{mm} yields the largest values of characteristic length with values ranging from 97 nm up to 254 nm. These three metrics span a factor of 2 or 3, indicating that though the distributions of these daughter fractions are narrower than the parent, they are still polydisperse.

A key advantage of ES-DMA is that it provides complete size distributions, not only ensemble average lengths such as light scattering. This enables us to quantify the breadth of the distributions. A simple measure of the width of the distribution is the FWHM, as given in Table 1. The separation by SEC reduces the width of the daughter distributions (FWHM = 46 nm to 123 nm) compared to the original distribution (see Figure 2c, with FWHM $\geq$ 400 nm), confirming the value of SEC in decreasing the polydispersity.
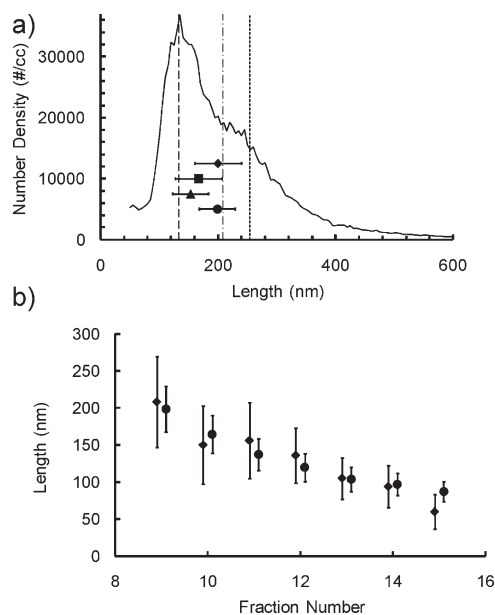
Figure 5. a) Length distribution of SWCNTs via ES-DMA with L_{mode} (long dash), L_{ave} (dash dot), and L_{mm} (short dash), and average lengths from FFF with UV/vis detection (circles), SEC MALS (triangles) using a rodlike data-fitting procedure, AFM (squares), and DLS (diamonds) for fraction 9. b) Number-average length, L_{ave}, determined by ES-DMA (diamonds) compared to average length ranges determined by FFF with UV/vis detection (circles) of SWNCT fractions 9 to 15. Fraction number is slightly offset to improve visibility of uncertainties, as described in the text.

2.3. Comparison to Other Techniques

We now compare the results of ES-DMA with those obtained using other sizing techniques for the same SEC fractions. For instance, Figure 5a plots the ES-DMA distribution for fraction 9 along with lengths determined by AFM,[2,13,15] MALS,[2,9,13,14] DLS,[13] and FFF with UV/vis detection.[13] The error bars represent 20% of the mean for optical methods (i.e., MALS and DLS), one standard deviation for AFM, and the range of values from rheological models for FFF. All of these measurements of SWCNT length fall within the central area of the distribution from ES-DMA, confirming the validity of the conversions used to transform raw ES-DMA data into length distributions. Figure 5b compares L_{ave} from ES-DMA (error bar represents one half of FWHM) with the FFF values for fractions 9 to 15. The excellent agreement further validates the use of ES-DMA for measuring the size distributions of the smaller SEC fractions (i.e., SWCNTs shorter than about 250 nm).

We finally note that it is possible, in principle, to use ES-DMA as a separation technique in its own right. The advantage of using the DMA for size separation is that it should be possible to obtain separated fractions of SWNCTs with length distributions as narrow as a few nanometers. These SWCNTs can be diverted to an electrostatic deposition chamber where they may be deposited onto substrates for further analysis or as components of a device.[37] With the current electrospray set up (the rate-limiting component) and solution concentrations sufficiently dilute to guarantee a single nanotube per droplet (to

prevent spurious bundling), thousands of length-selected nanotubes could be deposited per hour.

3. Conclusion

We have obtained length distributions of SWCNTs dispersed in aqueous solution by electrospraying them and then separating the charged SWCNTs based on their charge-to-size ratio in the DMA. We have developed a model to convert DMA data into length distribution, accounting for the salt precipitated on the surface of the SWCNTs after electrospraying. The lengths obtained compare favorably with other methods including multiangle light scattering, dynamic light scattering, field flow fractionation with UV/vis detection, and atomic force microscopy. The primary advantage of ES-DMA for obtaining size distributions of SWCNTs is that it provides a rapid and direct read-out of nanotube length distributions with resolution only a few nanometers wide. This study suggests ES-DMA is useful for the study of aqueous suspensions of a variety of high-aspect-ratio nanomaterials.

4. Experimental Section

Materials: Aqueous dispersions of CoMoCat SWCNTs (Southwest Nanotechnologies Inc. Batch NI-6-A001 S-P95-02) were prepared in 0.2 mol L^{-1} NaCl, 0.04 mol L^{-1} Tris, and HCl to a pH of 7.0 as described in detail elsewhere[14] by conjugating them with 30-mer 5′-GT(GT)$_{13}$GT-3′ single-stranded DNA (Integrated DNA Technologies) at a concentration of 1 mg mL^{-1}, followed by centrifugation (2 h, 21000 g). SEC was performed using an Agilent 1200 pump with a SepaxCNT (SEC-2000 + SEC-1000 + SEC-300) column set. Centrifuged samples were filtered through a 0.45-μm filter and injected in 0.5 mL increments with a 0.5 mL min^{-1} flow rate. The mobile phase matched the dispersion buffer (0.2 mol L^{-1} NaCl, 0.04 mol L^{-1} Tris, and HCl to a pH of 7.0). Several fractions of SWCNTs were collected at 2 min intervals spanning the time range from before the maximum size exclusion limit to beyond the minimum size exclusion limit, of which fractions 9 through 15 are analyzed herein (see the Supporting Information regarding the optimal selection of fractions for ES-DMA analysis). Multiple identical runs of SEC were performed, and the resulting like fractions were concentrated and dialyzed to a lower salt concentration using forced dialysis against an ultrafiltration membrane to generate the final samples. Typically 100 μL of 2 mmol L^{-1} ammonia acetate was added to approximately 30 μL of each SWCNT fraction to generate a suspension amenable to electrospray and decrease the concentration of SWCNTs below 100 μg mL^{-1}.[9,30] These solutions were stored in 1.5 mL centrifuge vials.

Electrospray particle generation and DMA: Figure 1a represents a schematic diagram of our experimental system.[16] The electrospray was operated at voltages that resulted in a stable cone-jet ≈2.0 kV. The electrospray sheath gas consisted of 1.0 L min^{-1} of air and 0.2 L min^{-1} of CO$_2$. To avoid capillary clogging during the ES process,[38] a 40-μm capillary was chosen to measure unfractionated SWCNTs, while minimization of salt crusts was more important for the fractionated SWCNTs, necessitating the use of a 25-μm capillary (limitations discussed in the Supporting Information). In order to achieve sufficient resolution in the DMA measurements, the sheath flow of the DMA, Q_{sh}, was chosen to be 30 L min^{-1} for SEC-classified SWCNTs and 10 L min^{-1} for unclassified SWCNTs. The nitrogen sheath gas was not recycled but was fed directly into the DMA. The 1.0 L min^{-1} output from the DMA was supplemented by 0.5 L min^{-1} of high-efficiency particulate air (HEPA) filtered room air and then introduced to the CPC.

Atomic force microscopy: The sample for AFM shown in Figure 1 was prepared by using an electrostatic deposition system. Electrosprayed and charged (but not size classified) particles were diverted to the electrostatic deposition chamber with an applied voltage of −10 kV and flow rate of 1.5 L min^{-1}. AFM images were obtained using a XE-100 (PSIA) scanning probe microscope operated in non-contact mode. The topographic image was recorded at a scan rate of 1 Hz using a non-contact cantilever (PSIA) with a force constant of 42 N m^{-1} and resonant frequency of 320 kHz. Grain-analysis software (PSIA) was used to determine the mean height of the individual nanotube features within an image scan. Other AFM mentioned in the text was performed as described by others.[2,14]

Calculation of mobility diameter and length: The mobility diameter, d_m, can be calculated from the DMA geometry and the flow conditions with

$$\frac{d_m}{C_c(d_m)} = \frac{2neV_{DMA}L_{DMA}}{3\mu\left[Q_{sh} + \frac{1}{2}Q_\alpha - \frac{1}{2}Q_s\right]\ln(r_o/r_i)}, \quad (5)$$

where

$$C(d_m) = 1 + \frac{2\lambda}{d_m}\left[1.257 + 0.400\cdot\exp\left(-\frac{1.110d_m}{2\lambda}\right)\right] \quad (6)$$

and n is the number of charges on the particles of magnitude e (1.602·10^{-19} C), V_{DMA} is the applied voltage in the differential mobility analyzer, L_{DMA} is its length (4.987 cm), r_i and r_o are the inner (0.937 cm) and outer diameter (1.905 cm) of the DMA column, respectively, λ is the mean free path of nitrogen (66 nm), μ is its viscosity (1.78·10^{-5} Pa s), Q_{sh} is the sheath flow entering the DMA, Q_a is the polydispersed inlet flow from the electrospray to the DMA, and Q_s is the monodisperse outlet flow from DMA to CPC. The length of a SWCNT, L_{nt}, was calculated as follows. In prior work Kim et al.[20,22,23] reported a relationship for the calculation of the gas-phase electrical mobilities of nanowires and subsequently the corresponding physical lengths based on the DMA conditions used

$$L_{nt} = A_1/(A_3 d_{nts}) - A_2 d_{nts}/A_3 \quad (7)$$

where $A_1 = [(2 e \lambda)/(\pi\mu)][(2\pi V_{DMA} L_{DMA})/([Q_{sh} + (Q_a\text{-}Q_s)/2]\ln[r_o/r_i])]$, $A_2 = (\pi f_{ac}/6 + 4/3)$, $A_3 = f_{ac} + [2 - (6 - \pi)f_{ac}/4)] \sin^2(1 \text{ rad})$, f_{ac} is the momentum accommodation coefficient (i.e., the fraction of nitrogen molecules reflecting off the nanotube in a diffuse manner, $f_{ac} = 0.9$), and d_{nts} is the apparent diameter of SWCNTs. We chose 1 rad for the argument of the sine function as this corresponds to random orientation within the DMA for these shorter SWCNTs. Though there is some uncertainty in accommodation coefficients reported in the literature, it does not significantly impact upon the results described herein.

The actual diameter of the nanotube, d_{nt}, differs from its apparent diameter, d_{nts}, due to the presence of non-volatile salts

that dry into a cylindrical shell on the surface of the SWCNT. Similar to the work of Kaufman[32] and Song et al.,[18] we construct a volume balance, which simplifies to

$$d_{nts}^2 = d_{nt}^2 + 2\,d_s^3(3L_{nt}) \tag{8}$$

This equation is based on three suppositions: 1) the volume of a nanotube is negligible relative to the volume of an electrosprayed droplet, hence the salts in droplets with or without SWCNTs reduce to the same volume of $\pi d_s^3/6$ after solvent evaporation, 2) following evaporation, the salt forms a uniform (right) cylindrical coating on the outer surface of SWCNTs, and 3) the relative increase in a SWCNT's length due to the coating shell is negligible compared to the change in diameter.

Equations (7) and (8) may be solved simultaneously for L_{nt} and d_{nts} by combining them into

$$B_1\,L_{nt}^4 + B_2\,L_{nt}^3 + B_3\,L_{nt}^2 + B_4\,L_{nt} + B_5 = 0 \tag{9}$$

where $B_1 = d_{nt}^2$, $B_2 = 2d_s^3/3$, $B_3 = -[(A_1 - A_2\,d_{nt}^2)/A_3]^2$, $B_4 = 4\,A_2\,d_s^3$ $(A_1 - A_2\,d_{nt}^2)/(3A_3^2)$, $B_5 = -[2A_2\,d_s^3/(3\,A_3)]^2$. This equation was then solved numerically with a Newton–Raphson method using a 0.1-nm or smaller step size. The DNA-coated diameter, d_{nt}, is estimated to be 2.0 nm based on the CoMoCat's diameter ($\approx$1.2 nm) and DNA coating (approximately 0.2 nm to 0.6 nm in radial thickness). By using a single diameter value, we implicitly suppose the absence of nanotube bundles, which, though commonly observed in SWCNT solutions, are greatly ameliorated by the DNA wrapping.[39] Of the four roots to Equation (9), only one was found to be real, positive, and definite and produced $d_{nts} > d_{nt}$. In all figures the gas-phase number density is plotted against this root for L_{nt} to provide length distributions.

Reference to commercial equipment or supplies does not imply its endorsement by the National Institute of Standards and Technology (NIST) nor implies it to necessarily be the best suited for its purpose.

[1] R. H. Baughman, A. A. Zakhidov, W. A. de Heer, Science 2002, 297, 787.

[2] J. A. Fagan, J. R. Simpson, B. J. Bauer, S. H. D. Lacerda, M. L. Becker, J. Chun, K. B. Migler, A. R. H. Walker, E. K. Hobbie, J. Am. Chem. Soc. 2007, 129, 10607.

[3] N. W. S. Kam, H. J. Dai, J. Am. Chem. Soc. 2005, 127, 6021.

[4] N. W. S. Kam, M. O'Connell, J. A. Wisdom, H. J. Dai, Proc. Natl. Acad. Sci. USA 2005, 102, 11600.

[5] D. Pantarotto, J. P. Briand, M. Prato, A. Bianco, Chem. Commun. 2004, 16.

[6] A. Bianco, K. Kostarelos, C. D. Partidos, M. Prato, Chem. Commun. 2005, 571.

[7] K. Kostarelos, L. Lacerda, G. Pastorin, W. Wu, S. Wieckowski, J. Luangsivilay, S. Godefroy, D. Pantarotto, J. P. Briand, S. Muller, M. Prato, A. Bianco, Nat. Nanotechnol. 2007, 2, 108.

[8] R. Singh, D. Pantarotto, L. Lacerda, G. Pastorin, C. Klumpp, M. Prato, A. Bianco, K. Kostarelos, Proc. Natl. Acad. Sci USA 2006, 103, 3357.

[9] M. L. Becker, J. A. Fagan, N. D. Gallant, B. J. Bauer, V. Bajpai, E. K. Hobbie, S. H. Lacerda, K. B. Migler, J. P. Jakupciak, Adv. Mater. 2007, 19, 939.

[10] P. W. Barone, S. Baik, D. A. Heller, M. S. Strano, Nat. Mater. 2005, 4, 86.

[11] A. M. Thayer, Chem. Eng. News 2007, 85, 29.

[12] W. D. Callister, Materials Science and Engineering: An Introduction, Wiley, New York 1994.

[13] J. Chun, J. A. Fagan, E. K. Hobbie, B. J. Bauer, Anal. Chem. 2008, 80, 2514.

[14] B. J. Bauer, J. A. Fagan, E. K. Hobbie, J. Chun, V. Bajpai, J. Phys. Chem. C 2008, 112, 1842.

[15] B. J. Bauer, M. L. Becker, V. Bajpai, J. A. Fagan, E. K. Hobbie, K. Migler, C. M. Guttman, W. R. Blair, J. Phys. Chem. C 2007, 111, 17914.

[16] L. F. Pease, D. H. Tsai, R. A. Zangmeister, M. R. Zachariah, M. J. Tarlov, J. Phys. Chem. C 2007, 111, 17155.

[17] D.-H. Tsai, R. A. Zangmeister, L. F. Pease, M. J. Tarlov, M. R. Zachariah, Langmuir 2008, 24, 8483.

[18] D. K. Song, I. W. Lenggoro, Y. Hayashi, M. Okuyama, S. S. Kim, Langmuir 2005, 21, 10375.

[19] B. E. Dahneke, J. Aerosol Sci. 1973, 4, 147.

[20] S. H. Kim, G. W. Mulholland, M. R. Zachariah, J. Aerosol Sci. 2007, 38, 823.

[21] S. H. Kim, M. R. Zachariah, J. Phys. Chem. B 2006, 110, 4555.

[22] S. H. Kim, M. R. Zachariah, Nanotechnology 2005, 16, 2149.

[23] S. H. Kim, M. R. Zachariah, Mater. Lett. 2007, 61, 2079.

[24] A. Moisala, A. G. Nasibulin, S. D. Shandakov, H. Jiang, E. I. Kauppinen, Carbon 2005, 43, 2066.

[25] R. A. Zangmeister, J. E. Maslar, A. Opdahl, M. J. Tarlov, Langmuir 2007, 23, 6252.

[26] A. Wiedensohler, J. Aerosol Sci. 1988, 19, 387.

[27] H. Y. Wen, G. P. Reischl, G. Kasper, J. Aerosol Sci. 1984, 15, 89.

[28] M. Zheng, A. Jagota, E. D. Semke, B. A. Diner, R. S. McLean, S. R. Lustig, R. E. Richardson, N. G. Tassi, Nat. Mater. 2003, 2, 338.

[29] M. Zheng, A. Jagota, M. S. Strano, A. P. Santos, P. Barone, S. G. Chou, B. A. Diner, M. S. Dresselhaus, R. S. Mclean, G. B. Onoa, G. G. Samsonidze, E. D. Semke, M. Usrey, D. J. Walls, Science 2003, 302, 1545.

[30] L. F. Pease, J. T. Elliott, D.-H. Tsai, M. R. Zachariah, M. J. Tarlov, Biotechnol. Bioeng. 2008, 101, 1214.

[31] P. H. M. Bottger, Z. Bi, D. Adolph, K. A. Dick, L. S. Karlsson, M. N. A. Karlsson, B. A. Wacaser, K. Deppert, Nanotechnology 2007, 18.

[32] S. L. Kaufman, Anal. Chim. Acta 2000, 406, 3.

[33] S. F. Wong, C. K. Meng, J. B. Fenn, J. Phys. Chem. 1988, 92, 546.

[34] J. B. Fenn, M. Mann, C. K. Meng, S. F. Wong, C. M. Whitehouse, Science 1989, 246, 64.

[35] N. A. Fuchs, Geofis. Pura Appl. 1963, 56, 185.

[36] H. Y. Wen, G. P. Reischl, G. Kasper, J. Aerosol Sci. 1984, 15, 103.

[37] D. H. Tsai, T. Hawa, H. C. Kan, R. J. Phaneuf, M. R. Zachariah, Nanotechnology 2007, 18.

[38] J. H. Kim, G. W. Mulholland, S. R. Kukuck, D. Y. H. Pui, J. Res. Natl. Inst. Stand. Technol. 2005, 110, 31.

[39] J. A. Fagan, B. J. Landi, I. Mandelbaum, J. R. Simpson, V. Bajpai, B. J. Bauer, K. Migler, A. R. H. Walker, R. Raffaelle, E. K. Hobbie, J. Phys. Chem. B 2006, 110, 23801.